Rapid switch-like sea ice growth and land ice−sea ice hysteresis

Roiy Sayag and Eli Tziperman

Environmental Sciences, Weizmann Institute, Rehovot, Israel

Department of Earth and Planetary Sciences and Division of Engineering and Applied Sciences, Harvard University, Cambridge, Massachusetts, USA

Michael Ghil

Département Terre-Atmosphère-Océan and Laboratoire de Météorologie Dynamique, Ecole Normale Supérieure, Paris, France

Department of Atmospheric Sciences and Institute of Geophysics and Planetary Physics, University of California, Los Angeles, California, USA

[1]   Rapid and extensive growth of sea ice cover was suggested to play a major role in the sea ice switch mechanism for the glacial cycles as well as on shorter millennial scales [*Gildor and Tziperman*, 2000]. This mechanism also predicts a hysteresis between sea ice and land ice, such that land ice grows when sea ice cover is small and withdraws when sea ice cover is more extensive. The switch-like sea ice growth and the hysteresis were previously demonstrated using a simple, highly idealized box model. In this work we demonstrate a switch-like sea ice behavior as well as the sea ice−land ice hysteresis using a coupled climate model that is continuous in the latitudinal dimension. It is shown that the switch-like sea ice growth occurs when the initial meridional atmospheric temperature gradient is not too strong. It is also shown that the meridional extent to which sea ice grows in a switch-like manner is not affected by the intensity of the thermohaline circulation, which does, however, influence the climate cooling that is needed to trigger such rapid sea ice growth.   *INDEX TERMS:* 3344 Meteorology and Atmospheric Dynamics: Paleoclimatology; 4215 Oceanography: General: Climate and interannual variability (3309); 4532 Oceanography: Physical: General circulation; 4540 Oceanography: Physical: Ice mechanics and air/sea/ice exchange processes; *KEYWORDS:* glacial cycles, sea ice, hysteresis

1. Introduction

[2] The last glacial period, from 15 to 60 kyr B.P., was characterized by numerous large-amplitude switches between cold and warm climates [*Heinrich*, 1988; *Bond et al.*, 1992; *Dansgaard et al.*, 1984]. Abrupt changes in the thermohaline circulation (THC) were shown to result in rapid climate change in many model studies [*Weaver et al.*, 1991; *Marotzke*, 2000]. More specifically, the atmospheric temperature signal of the Heinrich events and Dansgaard-Oeschger (DO) oscillations was attributed to large-amplitude changes in the THC [*Ganopolski and Rahmstorf*, 2001]. The present-day THC may be close to an instability threshold, beyond which it may show large-amplitude variability [*Tziperman et al.*, 1994; *Tziperman*, 1997]. However, explaining the large-amplitude temperature changes during Heinrich and DO events using the THC alone requires what seems to be unlikely large THC changes. The argument against a purely THC mechanism for Heinrich and DO events is strengthened by indications that the THC by itself may not have a sufficiently dominant

effect on the North Atlantic climate [*Seager et al.*, 2002; *Kerr*, 2002].

[3] Alternatively, it has been suggested that these large-scale atmospheric temperature changes could be explained by abrupt sea ice melting and expansion, due to its efficient cooling ice-albedo feedback [*Dansgaard et al.*, 1989; *Adams et al.*, 1999; *Gildor and Tziperman*, 2000, 2001; *Broecker*, 2000]. Abrupt expansion and melting of sea ice were also proposed to play a significant role in the dynamics of the 100 kyr cycles via the sea ice switch (SIS) glacial cycle mechanism of *Gildor and Tziperman* [2000, 2001]. As land ice slowly grows in this mechanism, it cools the atmosphere and ocean via its albedo effect. As the ocean reaches the freezing temperature, sea ice rapidly grows to a large spatial extent. Then land ice withdraws while the sea ice cover is extensive, and eventually, sea ice melts as well. The above description indicates that there is, in fact, a hysteresis effect between sea ice and land ice (Figure 1). By hysteresis it is meant that sea ice response to land ice extent is different for growing and withdrawing land ice phases (Figure 1). Sea ice acts in this proposed mechanism as a "switch" of the climate system, switching it from a growing ice sheet mode, where sea ice cover is relatively small, to a deglaciation mode, where sea ice cover is extensive. The sea ice−land ice hysteresis is perhaps the most important
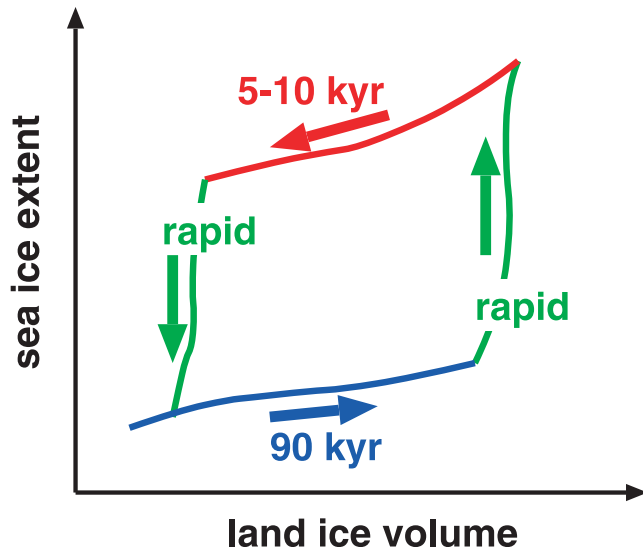
Figure 1. A schematic figure of the hysteresis between land ice and sea ice during glacial cycles, predicted using a simple box model by *Gildor and Tziperman* [2000] and examined here using a model that is continuous in the meridional direction.

prediction of the SIS mechanism in the sense that it may be the one most accessible to a possible future validation using proxy data.

[4] These rapid cycles of sea ice expansion and melting, as well as the above mentioned hysteresis, were found in a box model in which the entire surface ocean area, from 45°N to the pole, was represented by a single ocean box of uniform temperature. As soon as the polar box's temperature fell below the freezing temperature, sea ice started accumulating, covering nearly the entire surface within a few decades. This naturally leads to the question of whether the switch-like behavior of the sea ice in this model is merely an artifact of having a single box and a single temperature that represents the entire ocean north of 45°N.

[5] The purpose of this paper is to examine if the switch-like behavior of sea ice, as well as the sea ice–land ice hysteresis, is not an artifact of the coarse latitudinal resolution of the box model. We demonstrate a SIS behavior using a model that is continuous in the latitudinal dimension. We initialize our coupled model with different steady states that are characterized by different meridional temperature gradients in the atmosphere and ocean. For each of these steady states we then specify a slow growth of the land ice and observe the behavior of sea ice. We show that the sea ice indeed tends to grow rapidly (switch-like) when the land ice area crosses some threshold. The sea ice grows rapidly to a meridional extent which depends on the initial meridional temperature gradient in the ocean and the atmosphere. We also demonstrate that the extent to which the sea ice growth is rapid does not depend on the intensity of the THC. However, we find that the land ice cover that is needed to trigger the SIS does depend on the THC intensity. After the rapid, switch-like sea ice growth is completed, sea ice continues to grow slowly, together with the land ice. The land ice–sea ice hysteresis seen in this model is basically identical to that seen in the coarse box model of *Gildor and Tziperman* [2000, 2001].

[6] The switch-like growth and melting of sea ice presented and analyzed in the following sections and the corresponding climatic signal make this mechanism also a major candidate for explaining dramatic and abrupt climatic transitions such as Heinrich and DO events.

[7] Section 2 describes the model, while section 3 demonstrates the SIS behavior under various parameter regimes as well as a sea ice–land ice hysteresis. Sensitivity to model parameters is discussed in section 4, and concluding remarks follow in section 5.

2. Model Description

[8] Our model is composed of four coupled submodels for the ocean, atmosphere, sea ice, and land ice. It is continuous in the meridional direction and averaged in the zonal direction; it is basically a latitude-continuous version of the box model of *Gildor and Tziperman* [2001]. The fractions of land and ocean in a cell at a latitude y are $f_L(y)$ and $f_S(y)$, respectively, where $f_L(y) + f_S(y) = 1$. The fraction of land ice and sea ice in a given land or ocean cell are given by $f_{LI}(y)$ and $f_{SI}(y)$, respectively, where a value of 1 indicates a full coverage of the land or ocean cell by land ice or sea ice. There are two landmasses, one each in the Northern and Southern Hemispheres, as shown in Figure 2.

[9] The southern continent, representing Antarctica, occupies 10% of the total surface and is assumed to be permanently covered with ice. The present study is not concerned with possible changes to the Antarctic ice sheet or sea ice, although these could clearly also interact with their counterparts in the Northern Hemisphere. The northern continent, which occupies 23% of the total surface, contains an ice sheet that is free to grow. The atmospheric model is composed of one vertically integrated layer, representing the troposphere. The ocean has the same resolution as the atmosphere in the latitudinal coordinate and is composed of two vertical layers with thicknesses Δ_{top} and Δ_{bot} for the top and bottom ocean, respectively. Sea ice area is free to grow continuously within each ocean cell.

[10] There are n latitudinal cells with grid resolution of $\Delta y = \pi R_o/n$, where R_o is the Earth radius. The longitudinal extent is chosen to be $L_x = 4R_o$ such that the total surface area is equal to that of the spherical Earth, $4\pi R_o^2$. In our experiments the resolution is $\Delta y = 3°$ unless noted otherwise. The model equations are discretized in finite difference form and solved using a leapfrog scheme in time with temporal Robert filter coefficient $\gamma_R = 0.2$ for the ocean and ice and $\gamma_R = 0.39$ for the atmosphere [*Haltiner and Williams*, 1980].

[11] The above simplified geometry and limited physics clearly have their deficiencies. The rectangular geometry gives larger weight to the higher latitudes than the spherical geometry does. The north polar landmass and the specified fixed southern ice sheet are also clear deviations from reality. Yet these simplifications are used to isolate and study the properties of switch-like growth of sea ice more carefully under controlled circumstances.
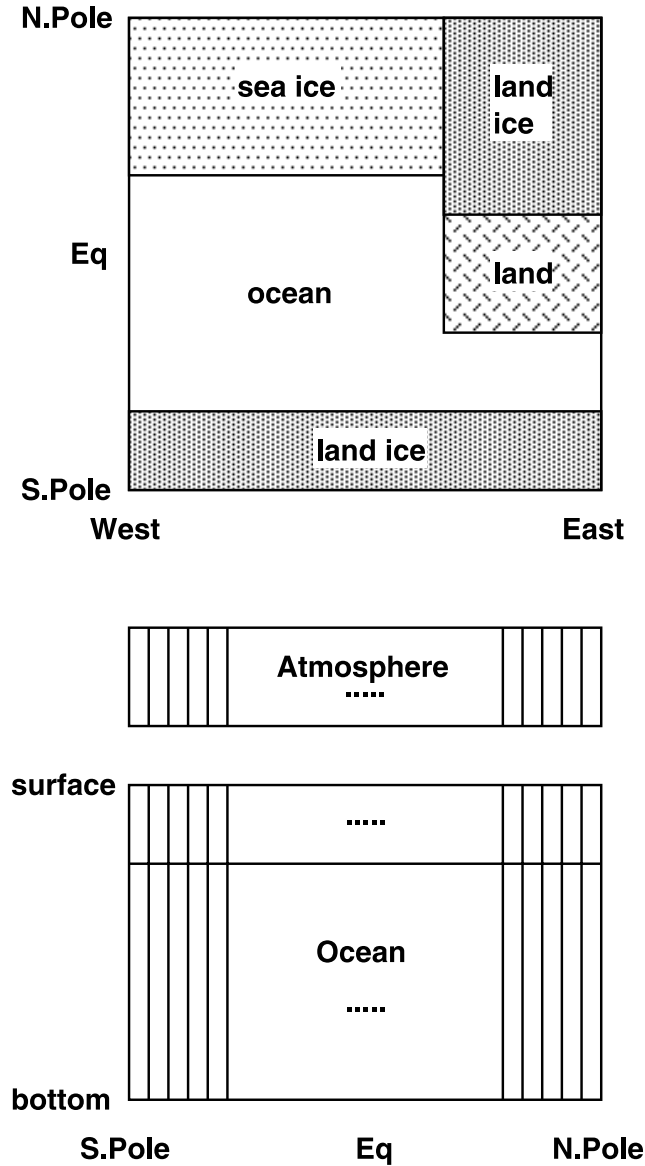
Figure 2. Model geometry. (top) Top view (latitude versus longitude) of the land, land ice, ocean, and sea ice distributions. (bottom) Latitude versus depth cross section through the ocean and atmosphere models. The vertical lines schematically mark a few of the grid boxes in the atmosphere and ocean. The latitudinal resolution (the latitudinal extent of these grid boxes) varies in the runs presented here from 6° to 1.5°.

[12] A detailed model description follows. Readers interested mostly in the model results may skip directly to section 3.

2.1. Atmospheric Model

2.1.1. Heat Equation

[13] The average potential atmospheric temperature at latitude y, represented by $\theta(y)$, is calculated by balancing the following heat fluxes: (1) incoming solar short-wave radiation (SW), (2) outgoing long-wave radiation (LW), (3)

meridional heat transport, and (4) heat exchange with the ocean. The equation for $\theta(y)$ is thus [*Marotzke and Stone*, 1995; *Rivin and Tziperman*, 1997; *Gildor and Tziperman*, 2001]

$$\frac{\partial \theta(y)}{\partial t} = \frac{2^{R/C_p^{\text{air}}} g}{P_o C_p^{\text{air}}} \{ H_{\text{land}}^{\text{SW}}(y) - H^{\text{LW}}(y)$$

$$- H_{\text{air-sea}}(y) + \frac{\partial}{\partial y} F_{\text{merid}}(y) \}, \quad (1)$$

where P_o is the atmospheric pressure at sea level, R is the gas constant for dry air, C_p^{air} is the air specific heat at constant pressure, g is the gravitational acceleration, and F_{merid} is meridional net heat transport.

[14] For the purpose of the present study the model is forced with annual mean solar radiation, neglecting seasonal and orbital variations. Part of the incoming SW radiation is reflected back to space owing to the atmospheric albedo, $\alpha_{\text{atm}}^{\text{SW}}$, and the rest is transmitted through the atmosphere to the surface. The incident radiation over land and ice sheets is partly reflected owing to their albedos (α_L^{SW} and $\alpha_{\text{LI}}^{\text{SW}}$), and the rest is assumed to be absorbed by the atmosphere. Thus the fraction of SW radiation that is absorbed and heats the atmosphere is

$$H_{\text{land}}^{\text{SW}}(y) = S_\odot [s_1 + s_2 \cos(y)] (1 - \alpha_{\text{atm}}^{\text{SW}})$$

$$\cdot \{ f_L(y) (1 - \alpha_L^{\text{SW}}) + f_{\text{LI}}(y) (1 - \alpha_{\text{LI}}^{\text{SW}}) \}, \quad (2)$$

where $S_\odot$ is the solar constant and s_1 and s_2 are chosen so that the annual average values of the incoming SW radiation at the equator and the poles are 430 W m^{-2} and 180 W m^{-2}, respectively [*Gill*, 1982]. The other part of the transmitted SW radiation, which contributes directly to the heating of the ocean and sea ice, is given by equations (15) and (19).

[15] The ocean-atmosphere heat exchange term, representing the sensible, latent, and radiative heat fluxes, as well as taking into account the insulating effect of sea ice [*Bryan et al.*, 1974], is given by

$$H_{\text{air-sea}}(y) = \frac{\rho_o C_p^{\text{water}} \Delta_{\text{top}}}{\tau} [\theta(y) - T(y)]$$

$$\cdot \left[f_{\text{open ocean}}(y) + f_{\text{SI}}(y) \frac{\gamma}{D_{\text{SI}}(y) + 1.7\text{m}} \right], \quad (3)$$

where C_p^{water} is the specific heat capacity of ocean water, T is the ocean's temperature, $f_{\text{open ocean}}$ is the fraction of open water, D_{SI} is sea ice thickness (in meters), and γ represents the insulating effect of sea ice. The restoring timescale τ, is chosen such that the air-sea heat flux to the atmosphere over the area from 45°N–90°N during an interglacial period is around 1.5 PW.

[16] The outgoing LW radiation, $H^{\text{LW}}(y)$, is

$$H^{\text{LW}}(y) = \sigma_{\text{SB}} \varepsilon(y) \theta^4(y), \quad (4)$$

where σ_{SB} is the Stephan-Boltzmann coefficient and $\varepsilon(y)$ is the atmospheric emissivity, which is prescribed to have a

Table 1. Atmospheric Model Parameters

Parameter	Value	Units
R, R_v	287.04, 461.5	J (kg $^\circ$K)$^{-1}$
C_p^{air}, C_p^{water}	1004, 3986	J (kg $^\circ$K)$^{-1}$
$\alpha_{atm}^{SW}, \alpha_L^{SW}, \alpha_{LI}^{SW}$	0.28, 0.1, 0.65	–
$S_\odot$	1365	W m^{-2}
R_o	6371×10^3	m
s_1, s_2	0.1319, 0.1832	–
v_H	10	m s^{-1}
C_w	1.24×10^{-3}	–
e_s^∞	2.525×10^{11}	Pa
L_e	2.501×10^6	J kg^{-1}
K_1, K_2	$2 \times 10^{14}; 8 \times 10^{18}$	m^4 (s $^\circ$K)$^{-1}$; m^5(s $^\circ$K^2)$^{-1}$
U	0.77	–

parabolic profile in latitude,

$$\varepsilon(y) = \frac{\varepsilon_N + \varepsilon_S - 2\varepsilon_o}{2|y_{max}|^2}y^2 + \frac{\varepsilon_N - \varepsilon_S}{2|y_{max}|}y + \varepsilon_o,$$

where $|y_{max}|$ is 90° and ε_N, ε_S, and ε_o are the emissivities at the North Pole, South Pole, and equator, respectively. The emissivity, $\varepsilon(y)$, is taken to be constant in time, neglecting the effect of variable atmospheric cloud cover, humidity, aerosol concentration, or CO_2 [*Gildor and Tziperman*, 2001].

[17] The meridional net heat transport, F_{merid}, in equation (1) is based on the parameterization of *Stone* [1990]:

$$F_{merid}(y) = C\left(C_1 + C_2\left|\frac{\partial\theta(y)}{\partial y}\right|\right)\frac{\partial\theta(y)}{\partial y}, \qquad (5)$$

where

$$C_1 = 10^{19}\frac{J}{s^o K} \qquad C_2 = 5 \times 10^{25}\frac{J(m)}{s^o K^2}.$$

The coefficient C_1 was chosen to be the smallest value that eliminates the numerical noise generated where the non-linear diffusivity $C_2|\partial\theta(y)/\partial y|$ vanishes, while C_2 and C (a nondimensional coefficient of order 1) were chosen such that the maximum meridional heat flux during an interglacial is $\sim$5 PW [*Trenberth and Caron*, 2001]. All atmospheric model parameters are given in Table 1.

2.1.2. Moisture Equation

[18] The equation for atmospheric humidity content, $q(y)$, includes evaporation from the ocean and meridional humidity exchange,

$$\frac{\partial q(y)}{\partial t} = \frac{g\rho_{water}}{P_o}\left\{E(y) + \frac{1}{L_x}\frac{\partial}{\partial y}F_{Mq}(y)\right\}, \qquad (6)$$

where ρ_{water} is the water density. The evaporation E at latitude y, proportional to the difference between the saturation specific humidity at the ocean level and the specific atmospheric humidity, is thus

$$E(y) = C_w v_H \frac{\rho_{air}}{\rho_{water}}\left\{q_s^T(y) - q(y)\right\}f_{open\,ocean}(y); \qquad (7)$$

here v_H is a horizontal wind velocity scale, C_w is the drag coefficient chosen such that the average $E - P$ over the latitudes 45°–90°N during an interglacial is about -0.2 m yr^{-1} [*Peixoto and Oort*, 1991], P is precipitation, and the saturation specific humidity at the ocean level, denoted by q_s^T, is calculated by the Clausius Clapeyron equation

$$q_s^T(y) = 2\left(0.622 e_s^\infty/P_o\right)e^{-L_e/[R_v T(y)]}, \qquad (8)$$

where e_s^∞ is water vapor saturation pressure, R_v is the water vapor gas constant, and L_e is the latent heat of evaporation for water.

[19] The meridional moisture transport parameterization is similar to the meridional heat flux parameterization

$$F_{Mq}(y) = \left(K_1 + K_2\left|\frac{\partial\theta(y)}{\partial y}\right|\right)\frac{\partial q(y)}{\partial y}, \qquad (9)$$

where K_2 is chosen such that the maximal meridional moisture flux in the Northern Hemisphere during an inter-glacial is $F_{Mq}^{max} \sim 0.5$ sverdrup (Sv) $(1 \text{ Sv} = 10^6 \text{ m}^3 \text{ s}^{-1})$, while K_1 is chosen again such that numerical noise is eliminated.

[20] A maximum atmospheric relative humidity, U, is specified such that the maximum atmospheric humidity is

$$q_{max}(y) = Uq_s^\theta(y). \qquad (10)$$

Any humidity excess is released as precipitation, P, which is therefore given by

$$P(y) = \begin{cases} \dfrac{P_o}{g\rho_{water}}\dfrac{1}{\Delta t}[q(y) - q_{max}(y)] & q(y) > q_{max}(y) \\ 0 & \text{otherwise} \end{cases}, \qquad (11)$$

where Δt is the model time step. Precipitation above land and land ice is assumed to run off to the ocean to be part of the freshwater flux, together with precipitation over the ocean, while precipitation above sea ice accumulates as ice.

2.2. Ocean Model

[21] The meridional mass transport across a given latitude in the top ocean layer is calculated from the meridional density gradient of the four adjacent cells, as done for a four-box Stommel-like model [*Stommel*, 1961; *Huang et al.*, 1992],

$$v_{top}(y) = \frac{g\Delta_{bot}}{2r_o\Delta y(\Delta_{top} + \Delta_{bot})\rho_o}$$
$$\cdot\left\{\Delta_{top}\left[\rho_{top}(y+1) - \rho_{top}(y)\right] + \Delta_{bot}[\rho_{bot}(y+1) - \rho_{bot}(y)]\right\}, \qquad (12)$$

where r_o is a Rayleigh friction coefficient. The vertical velocity w is calculated from the divergence of the meridional velocity using the continuity equation.

[22] The ocean temperature and salinity are governed by advection-diffusion equations, which employ centered differencing in the horizontal direction and upstream differencing for the vertical advection term. The temperature equation for the upper layer, for example, takes the form

$$\frac{\partial T_{\text{top}}}{\partial t} + \frac{\partial(v_{\text{top}} T_{\text{top}})}{\partial y} + \frac{w\widehat{T}}{\Delta_{\text{top}}} = K_y^T \frac{\partial^2 T_{\text{top}}}{\partial y^2} + \frac{1}{\Delta_{\text{top}}}$$
$$\cdot \left[K_z^T \frac{T_{\text{bot}} - T_{\text{top}}}{\frac{1}{2}(\Delta_{\text{top}} + \Delta_{\text{bot}})} + \frac{H_{\text{surface}}^T(y)}{\rho_o C_p^{\text{water}}} \right], \quad (13)$$

where $\widehat{T} = T_{\text{top}}$ if w is downward and $\widehat{T} = T_{\text{bot}}$ otherwise and K_y^T and K_z^T are the meridional and vertical diffusion coefficients, respectively. The surface heat flux is

$$H_{\text{surface}}^T(y) = H_{\text{air-sea}}(y) + H_{\text{ocean}}^{\text{SW}}(y) + \frac{\rho_{\text{sea ice}} L_f^{\text{SI}}}{L_x \Delta y}$$
$$\cdot \left\{ H_{\text{SI} \leftrightarrow \text{ocean}}(y) + H_{\text{SI}}^{\text{SW}}(y)(1 - \alpha_{\text{melting}}) \right\}, \quad (14)$$

where $H_{\text{air-sea}}$ is the ocean-atmosphere heat exchange term given by equation (3) and $H_{\text{ocean}}^{\text{SW}}$ is the solar SW radiation portion absorbed by the ocean; similarly to equation (2), the latter is given by

$$H_{\text{ocean}}^{\text{SW}}(y) = S_\odot [s_1 + s_2 \cos(y)](1 - \alpha_{\text{atm}}^{\text{SW}}) \cdot \left\{ f_s(y)(1 - \alpha_S^{\text{SW}}) \right\}. \quad (15)$$

The last two terms in the curly brackets in equation (14) are discussed in more detail in section 2.3; they are due to the melting and formation of sea ice and solar SW radiation over sea-ice-covered ocean regions.

[23] The ocean salinity, S, varies owing to evaporation and precipitation, water runoff from land ice sheets, and sea ice volume variations, as well as advection-diffusion and convection in the ocean. Its surface forcing is given by

$$H_{\text{surface}}^S(y) = \frac{S_o}{V_s(y)} \left\{ L_x \Delta y [E(y) - P(y)] + \frac{\partial V_{\text{SI}}(y)}{\partial t} \right\}, \quad (16)$$

where $V_s(y)$ is the top ocean layer volume at latitude y and $V_{\text{SI}}(y)$ is the sea ice volume at latitude y. Water runoff from Antarctica to the Southern Ocean is distributed homogeneously over the three southernmost oceanic cells to avoid an unrealistically strong freshwater flux into the single oceanic cell nearest Antarctica.

[24] We use a linear equation of state

$$\rho(T, S) = \rho_o - \alpha(T - T_o) + \beta(S - S_o), \quad (17)$$

where T_o, S_o, and ρ_o are reference ocean temperature, salinity, and density, while α and β are the thermal and

Table 2. Ocean Model Parameters

Parameter	Value	Units
Δ_{top}, Δ_{bot}	500, 5000	m
r_o	8×10^{-4}	s^{-1}
K_y^T, K_z^T, K_y^S, K_z^S	3×10^3, 10^{-4}, 3×10^3, 10^{-4}	$m^2 \, s^{-1}$
α_S	0.1	−
T_o	10	°C
S_o	35	ppt[a]
ρ_o	1026.952	kg m^{-3}
α	0.171	°kg m^{-3} K^{-1}
β	0.781	kg m^{-3}

[a]The abbreviation ppt stands for parts per thousand.

salinity expansion coefficients, respectively [*Gill*, 1982]. When water density in an upper ocean cell is larger than that of the corresponding cell at the deep ocean, convection is assumed to instantaneously mix salinity and heat between the two cells; this mixing makes the column's temperature, salinity, and density vertically homogeneous. The ocean model parameters are given in Table 2.

2.3. Sea Ice Model

[25] The sea ice cover in each ocean model grid cell is characterized by its thickness and its area fraction within the ocean cell. Sea ice area is assumed to initially grow continuously within a given ocean grid cell at a thickness of 3 m. Once the grid cell is completely sea ice covered, the sea ice thickness may increase further. The sea ice growth is also continuous in the latitudinal direction within each grid cell. As soon as sea ice appears in a given latitudinal grid cell, it can expand continuously within this cell until it is filled completely.

[26] The fraction of the ocean surface in cell y that is sea ice covered, $f_{\text{SI}}(y)$, is therefore determined from the total sea ice volume within this cell, $V^{\text{SI}}(y)$, such that its minimum thickness is 3 m; i.e.,

$$f_{\text{SI}}(y) = \frac{V^{\text{SI}}(y)}{L_x \Delta y 3\text{m}}.$$

Sea ice volume, in our model, varies owing to the following processes: (1) freezing/melting induced by heat exchanges with the ocean, (2) precipitation on sea ice, (3) melting due to solar SW radiation, and (4) diffusion of sea ice thickness across different latitudes.

[27] The value for minimum sea ice thickness that we use is consistent with the observed one in present-day climate in areas where sea ice cover varies with the seasonal cycle. The expansion rate of sea ice should not change significantly should we use a different initial sea ice thickness of the same order of magnitude. The expansion rate of sea ice is limited by the time it takes the ocean and atmosphere south of the sea ice margin to cool in response to newly formed sea ice. That is, the time it takes sea ice to freeze once ocean water is at freezing temperature is not a limiting factor. Furthermore, the heat required to freeze or melt a few meters of sea ice thickness is negligible relative to the heat required to change the temperature of the upper ocean level in order to continue the horizontal sea ice expansion.

[28] Sea ice is formed as soon as the ocean's temperature, T, drops below the threshold freezing temperature, T_{SI}; sea

Table 3. Sea Ice Model's Parameters

Parameter	Value	Units
$\rho_{\text{sea ice}}$	917	kg m^{-3}
L_f^{SI}	3.34×10^5	J kg^{-1}
$\tau_{\text{SI}}^{\text{SW}}$	1/24	year
$\alpha_{\text{sea ice}}$, α_{melting}	0.85, 0.2	–
K_{SI}	10^4	m^2 s^{-1}
T_{SI}	0	°C
γ	0.05	m

ice melts otherwise. The formation or melting rate is given by

$$H_{\text{SI}\leftrightarrow\text{ocean}}(y) = \frac{\rho_o C_p^{\text{water}}}{\tau_{\text{SI}}} \frac{V_s(y)}{\rho_{\text{sea ice}} L_f^{\text{SI}}} [T_{\text{SI}} - T(y)], \quad (18)$$

where $\rho_{\text{sea ice}}$ is the sea ice density and L_f^{SI} is the latent heat of fusion for sea ice. The sea ice relaxation timescale τ_{SI} is chosen to be short enough to ensure that $|T| \simeq T_{\text{SI}}$ when sea ice is present. The contribution of precipitation to the rate of sea ice growth is

$$P_{\text{sea ice}}(y) = P(y) L_x \Delta y f_{\text{SI}}(y),$$

where $P(y)$ is given by equation (11).

[29] SW radiation over sea-ice-covered ocean is partly reflected, is partly absorbed, and induces melting; the rest is transmitted to the ocean below. The sea ice albedo is denoted by $\alpha_{\text{sea ice}}^{\text{SW}}$, and the SW radiation fraction that is assumed to be absorbed by the sea ice and induces melting is denoted by α_{melting}. The SW radiation that is absorbed by sea ice or transmitted through it is given by

$$H_{\text{SI}}^{\text{SW}}(y) = S_\odot [s_1 + s_2 \cos(y)] \left(1 - \alpha_{\text{atm}}^{\text{SW}}\right)$$
$$\cdot \left(1 - \alpha_{\text{sea ice}}^{\text{SW}}\right) \frac{L_x \Delta y f_{\text{SI}}(y)}{\rho_{\text{sea ice}} L_f^{\text{SI}}}. \quad (19)$$

Finally, we include sea ice thickness diffusion in the meridional direction so that the equation for the sea ice volume is

$$\frac{\partial V_{\text{SI}}(y)}{\partial t} = P_{\text{sea ice}}(y) + H_{\text{SI}\leftrightarrow\text{ocean}}(y) - H_{\text{SI}}^{\text{SW}}(y)\alpha_{\text{melting}}$$
$$+ K_{\text{SI}} \frac{\partial^2 D_{\text{SI}}(y)}{\partial y^2} L_x \Delta y f_{\text{SI}}(y), \quad (20)$$

where K_{SI} is the sea ice diffusion constant. The sea ice model parameters are given in Table 3.

2.4. Land Ice Model

[30] Our ice sheet model is zonally uniform, assumes a flat bottom and perfect plasticity, and is therefore characterized by a parabolic height profile in the latitude [*Ghil and Treut*, 1981; *Paterson*, 1994; *Ghil*, 1994; *Gildor and*

Tziperman, 2001]. The glacier height, h, at distance, l, from its center is

$$h(l) = \sqrt{\frac{2\tau_o}{g\rho_{\text{LI}}}(L - |l|)}, \quad (21)$$

where $2L$ is the total extent of the glacier in the latitudinal direction, $|l| \leq L$, the stress threshold is τ_o, and the ice density is ρ_{LI}.

[31] For the purpose of the present paper we do not allow the ice sheet to vary freely owing to accumulation (precipitation) and ablation, but we prescribe the ice sheet volume to increase linearly in time at a constant rate, independent of the precipitation rate, and without affecting the model's water mass balance. Clearly, the effect of other atmospheric and oceanic feedbacks and the way they correlate with land ice growth rate is interesting and should be addressed in future work. Yet the specified behavior of the land ice sheets allows us to focus on the behavior of sea ice, which is the main objective of the present study. Hence the equation that governs the ice volume is

$$\frac{\text{dV}_{\text{land ice}}}{\text{dt}} = \text{LI}_{\text{source}}, \quad (22)$$

with a constant source/sink term $\text{LI}_{\text{source}}$.

[32] The southern ice sheet in our model is constrained to cover the entire southern continent, consistent with its behavior during the Pleistocene [*Crowley and North*, 1991]. The northern ice sheet, on the other hand, extends initially from the North Pole to ~65°N and grows according to equation (22). Land ice model parameters are given in Table 4.

2.5. Standard Model Simulation Results

[33] Before proceeding to the model experiments, we note that a "standard" glacial-like solution indicates that the model performs reasonably given its simplicity. Figure 3 shows the temperature, salinity, density, and meridional circulation in the ocean, as well as the atmospheric temperature and meridional heat flux, for a case where the northern ice sheet extends to 55°N and is specified to be fixed in time.

3. What Enables a Switch-Like Behavior of Sea Ice

[34] Our objective is to find out under what circumstances sea ice may grow suddenly during a slow climate cooling, enforced in our model by specifying a slowly growing ice sheet in the Northern Hemisphere, as explained in section 1. Over many model experiments that we have carried out, the main factor determining whether rapid, switch-like growth

Table 4. Ice Sheet Model Parameters

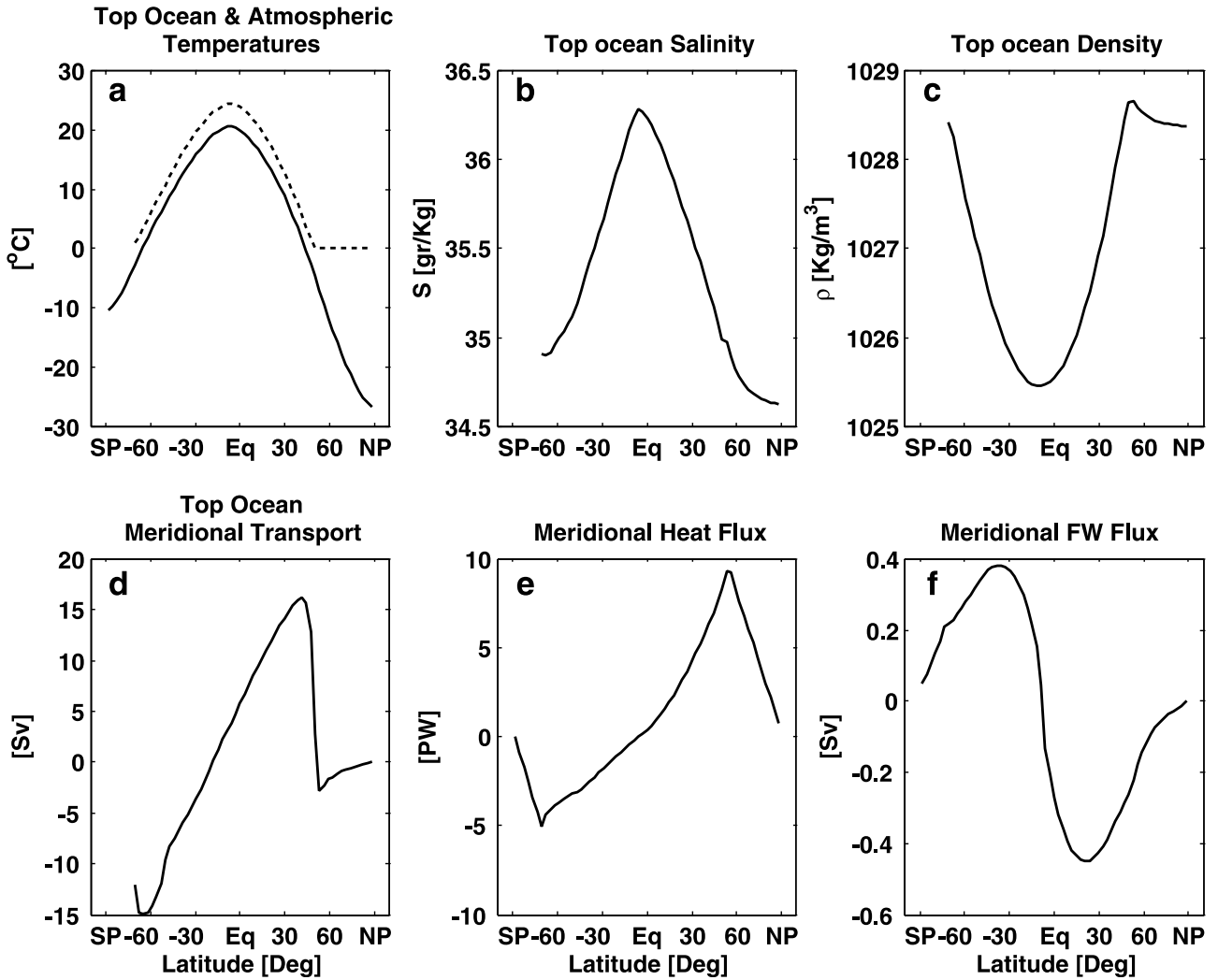| Parameter	Value	Units
ρ_{LI}	850	kg m^{-3}
τ_o	100	kPa

Figure 3. Model solution for typical glacial-like boundary conditions of northern ice sheet extending to 55°N. Shown as a function of latitude are (a) atmospheric temperature (solid line) and ocean top layer temperature (dashed line) in °C, (b) upper ocean salinity (parts per thousand), (c) density of the upper ocean layer (kg m^{-3}), (d) meridional transport in upper ocean (sverdrup (Sv)), (e) atmospheric meridional heat flux (PW), and (f) meridional atmospheric freshwater (FW) flux (Sv).

of sea ice is possible was the meridional temperature gradient in the ocean and atmosphere. In order to demonstrate this we first initialize our coupled model with three different steady states that have different meridional temperature gradients, and we examine the sea ice behavior as the land ice slowly grows. The three different steady state profiles of atmospheric temperature (Figure 4) are obtained by adjusting three factors: the atmospheric meridional heat flux coefficients (C), the THC (via the coefficient r_o), and the atmospheric latitudinal emissivity profile via (ε_S, ε_o, ε_N) (Table 5). The three initial conditions were obtained for a fixed-volume ice sheet (LI$_{source}$ = 0) that reaches a southernmost latitude of 66°N. A parameter set identical to initial condition 1 (IC 1) was used to generate the standard glacial solution shown in Figure 3.

[35] The three steady states in Figure 4 are characterized by atmospheric temperature profiles with different meridi-

onal temperature gradients, defined to be the temperature difference between the maximum at the lower latitudes and the averaged polar temperature, and are denoted as $\Delta\theta_{equil}$. The corresponding ocean's surface temperature throughout the model domain is above the freezing temperature, T_{SI}. We tuned the Rayleigh friction coefficient, r_0, to keep the maximum THC value at ~20 Sv (between 16 and 23 Sv) in order to isolate the role of meridional temperature gradient from that of the THC. The emissivity and meridional atmospheric heat flux parameters were chosen such that the polar temperatures for the three different steady states had the same values, $\theta_{NorthPole} \simeq -1°C$ and $\theta_{SouthPole} \simeq -9°C$. The separate roles of the THC intensity, the meridional atmospheric heat transport, and the emissivity are examined below. In section 4 we examine the sensitivity of the model behavior to horizontal resolution and some additional technical factors.
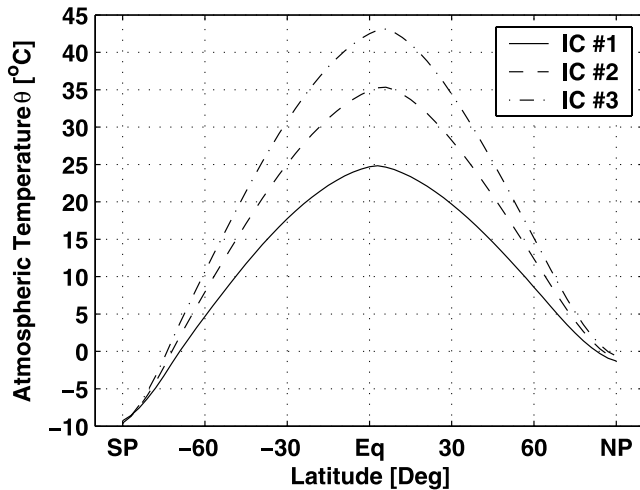
Figure 4. Three profiles of steady state atmospheric temperature (°C). These profiles were used as initial conditions (IC) for the model experiments examining the response of the sea ice to a slow equatorward expansion of the continental ice sheet. Each of the three steady states, denoted by IC 1 (solid line), IC 2 (dashed line), and IC 3 (dash-dotted line), was obtained for a particular set of model parameters, given in Table 5.

[36] The three steady states whose atmospheric temperature profiles are shown in Figure 4 were then used as initial conditions for the model runs with a specified growing northern ice sheet for an integration period of 100,000 years and ice sheet growth rate of $LI_{source} = 5 \times 10^4$ m^3 s^{-1}, which is equivalent to a reduction of ~39 m per 10,000 years in terms of real ocean level. The results of the model runs starting at the different initial conditions are shown in Figure 5.

[37] As the northern ice sheet grows in these model runs, the ocean is initially sea-ice-free. At some stage the increase in the surface albedo due to the growing ice sheet and the resulting atmospheric cooling bring the northernmost part of the polar ocean to the freezing point. This initiates sea ice formation. The high sea ice albedo reflects much of the incoming SW radiation to outer space, and furthermore, the insulating sea ice cover reduces the heat flux from the ocean to the atmosphere, resulting in a strong atmospheric cooling. This feedback leads to additional rapid sea ice expansion up to the maximum extent shown by the nearly vertical line segments in Figure 5. The high-latitude cooling and hence increased temperature gradient in the ocean induce a stronger THC and therefore a stronger meridional oceanic heat flux. Similarly, the high-latitude atmospheric cooling strengthens the meridional atmospheric heat flux. The stronger combined oceanic and atmospheric meridional heat flux, together with the insulating sea ice that prevents further cooling of the sea-ice-covered ocean area, eventually bring to a halt the sea ice expansion.

[38] As seen in Figure 5, the extent of the initial, switch-like, sea ice expansion is a strong function of the initial meridional temperature gradient in the ocean and the atmosphere. Note that after the rapid sea ice growth stops,

the sea ice continues to slowly expand as the land ice grows and as the climate cools. It is the switch-like growth of sea ice that is our main focus in this paper. Such rapid growth (and melts) may explain the rapid cooling and warming events during Heinrich and DO events [*Heinrich*, 1988; *Bond et al.*, 1992; *Dansgaard et al.*, 1984]. Additionally, the very rapid sea ice growth in Figure 5 supports the sea ice switch mechanism demonstrated by *Gildor and Tziperman* [2000] using a much simpler box model. Note, though, that the rapid sea ice expansion in Figure 5 lasts up to a thousand years, while in the box model of *Gildor and Tziperman* [2000], this growth lasted a few decades. Still, this expansion may be considered "switch-like" in both cases, given the much slower timescale of the 100 kyr glacial cycle.

[39] The three initial states used for the runs of Figure 5 were obtained by varying several model parameters that affect the THC, meridional atmospheric heat flux, and atmospheric emissivity. We now wish to understand the role of each of these factors separately in determining the meridional extent of the switch-like sea ice growth and the minimal land ice volume needed to trigger this switch-like expansion. For this purpose we next examine nine model experiments in which each of these parameters is varied separately. The relevant model runs are summarized in Table 6.

[40] When we vary the THC transport coefficient, r_o, the THC varies significantly (Table 6); yet because the meridional temperature gradient in the ocean and atmosphere does not vary strongly with the THC (Table 6), the effect of the THC transport coefficient on the SIS extent turns out to be relatively small (not shown here, but see *Sayag* [2003]). In contrast, the critical extent of land ice cover for which the switch-like growth starts does vary considerably with the THC (Figure 6b). A stronger THC corresponds to a larger oceanic meridional heat flux and hence to a slower cooling of the polar ocean as the land ice grows. This delay in ocean cooling allows the land ice cover to further increase before the rapid sea ice growth starts. Similarly, when varying the coefficient C which determines the atmospheric meridional heat flux, there is a significant effect on the critical land ice extent for which sea ice growth starts (Figure 6a); the basic reason is the same as that noted for Figure 6b.

[41] The set of experiments used to examine the separate roles of the THC, atmospheric meridional heat flux, and atmospheric emissivity (Table 6) may also be used to strengthen the conclusion regarding the role of the initial meridional temperature gradient in setting the extent of the switch-like sea ice growth. We collect the results of all the model runs described in Table 6, together with additional model experiments in which we varied some of the discussed parameters simultaneously (Table 5), and we plot the extent of the switch-like sea ice expansion as a function of

Table 5. Model Parameters for the Model Runs 1−3

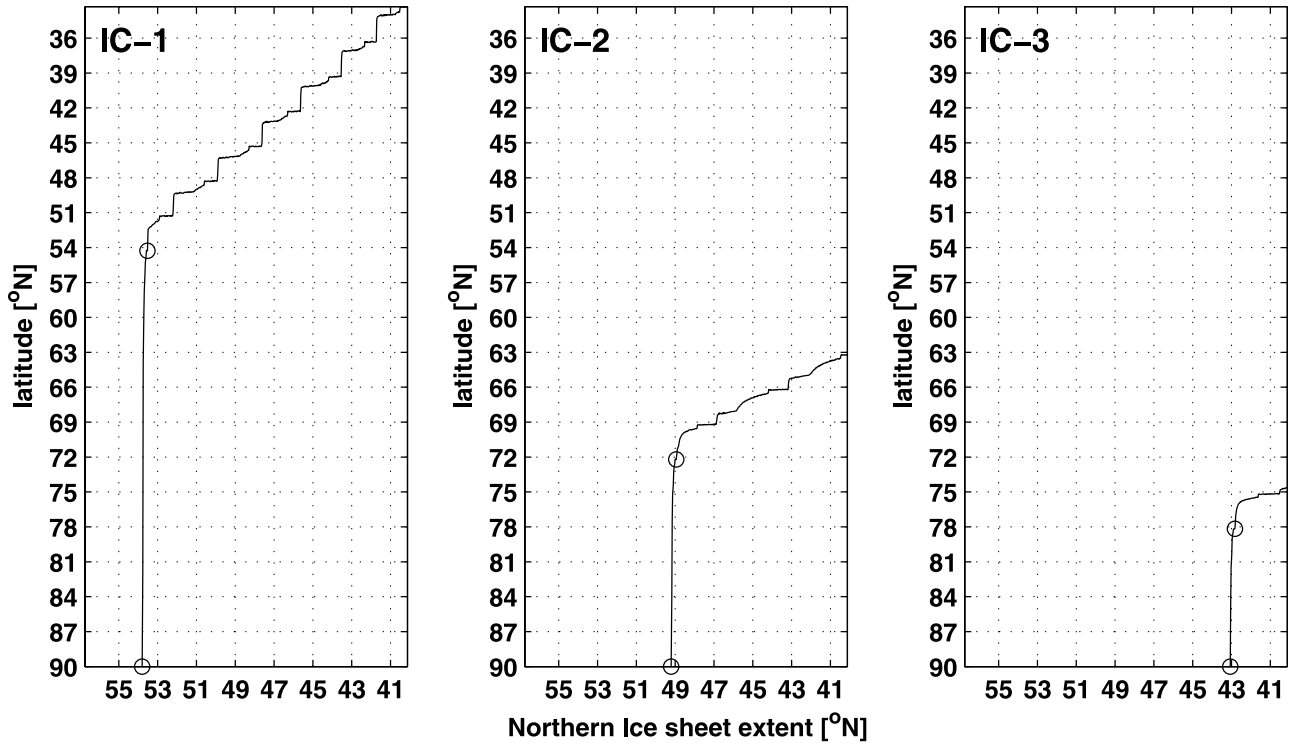| IC[a]	$\varepsilon_S, \varepsilon_o, \varepsilon_N$	C	r_o, s^{-1}	$\Delta\theta_{equil}$,°C
1	0.55, 0.55, 0.55	3.5	15	30.1
2	0.60, 0.46, 0.64	2.5	23	40.6
3	0.64, 0.40, 0.70	2	27	48.3

[a]IC stands for initial condition.

Figure 5. Results for the model runs with specified constant rate of ice sheet growth over a period of 100 kyr, starting with the three different initial conditions IC 1, IC 2, and IC 3 shown in Figure 4. Shown is the sea ice extent (southernmost ocean cell with sea ice) as a function of the land ice extent (the southernmost latitude to which the Northern Hemisphere ice sheet extends). The straight vertical segment in these plots corresponds to the rapid, switch-like sea ice growth. After the rapid growth, sea ice continues to expand slowly with the growing land ice. The two circles in each plot mark the beginning of the sea ice growth and 1000 years later. Therefore these two circles mark the time interval in which sea ice grows in a switch-like manner.

the initial atmospheric temperature gradient (Figure 7). Figure 7 clearly suggests that whether we change the meridional atmospheric temperature gradient by varying the emissivity, meridional heat fluxes, or the THC, the magnitude of the switch-like sea ice expansion is proportional to the initial value of the temperature gradient.

[42] The dependence of the meridional extent of sea ice switch-like growth on the meridional atmospheric (and hence oceanic) temperature gradient makes sense physically as well. For the sea ice cover to expand, the ocean water has to freeze. Once the expanding land ice cover cools the polar ocean to the freezing temperature, the rate at which additional equatorward ocean latitude bands cool down to freezing temperature depends on the meridional temperature gradient. A smaller meridional temperature gradient in the ocean implies that less cooling is required to bring a larger meridional extent of the ocean to the freezing temperature. Hence there is a larger extent of switch-like sea ice growth for smaller meridional temperature gradient.

[43] Perhaps the most important prediction of the SIS mechanism of *Gildor and Tziperman* [2000], in terms of possible future validation using proxy records, is the hysteresis of the sea ice and land ice. That is, as land ice sheets grow and retreat, the sea ice varies out of phase with land ice. In

order to examine whether this prediction also is robust with respect to the model's added detail and resolution, we ran a model experiment in which we initially slowly increased the Northern Hemisphere land ice extent and then slowly decreased it. Figure 8 shows that in our present model the land

Table 6. Varying the Atmospheric Meridional Heat Flux Coefficient, C, the Initial Thermohaline Circulation (THC) Intensity (Via the Coefficient r_0), and the Atmospheric Emissivity Profile One at a Time

IC	$\varepsilon_S, \varepsilon_o, \varepsilon_N$	C	r_o, s^{-1}	$\Delta\theta_{equil}$, °C
C_1	0.60, 0.46, 0.64	2.5	23	40.6
C_2	0.60, 0.46, 0.64	3.75	23	36.1
C_3	0.60, 0.46, 0.64	5	23	32.9
IC	$\varepsilon_S, \varepsilon_o, \varepsilon_N$	C	THC, Sv, Via r_o, s^{-1a}	$\Delta\theta_{equil}$, °C
r_{o1}	0.60, 0.46, 0.65	2.5	7.5 (14)	37.2
r_{o2}	0.60, 0.46, 0.65	2.5	15 (26)	39.8
r_{o3}	0.60, 0.46, 0.65	2.5	30 (46)	41.1
IC	$\varepsilon_S, \varepsilon_o, \varepsilon_N$	C	r_o, s^{-1}	$\Delta\theta_{equil}$, °C
ε_1	0.50, 0.56, 0.53	2.5	15	31.0
ε_2	0.60, 0.46, 0.65	2.5	15	39.8
ε_3	0.69, 0.37, 0.77	2.5	15	47.3

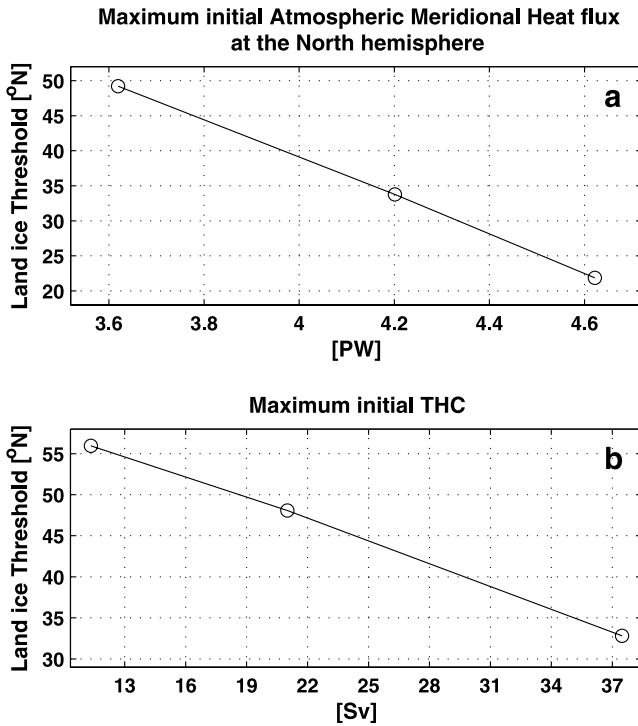[a]Values for r$_o$ are given in parentheses.

Figure 6. The critical northern ice sheet extent at which sea ice starts to grow (the latitude of the southern edge of the continental ice sheet, in degrees) as a function of the (a) maximum (over all latitudes) initial steady state atmospheric meridional heat (PW) for runs C_1–C_3 in Table 6 and (b) maximum (over all latitudes) of the initial steady state meridional thermohaline circulation (THC) (Sv), runs r_{o1}–r_{o3} in Table 6.

ice and sea ice show precisely the same hysteresis as is shown in the simple box model of *Gildor and Tziperman* [2000]. That is, sea ice grows initially when land ice reaches a latitude of 45°N but remains "on" when the land ice retreats back to 55°N. The term "hysteresis" basically refers to the fact that the responses of the sea ice to growing and shrinking land ice are different (growth and melting occur at different latitudes of the land ice). This is consistent with the suggestion of the SIS mechanism that sea ice extent during deglaciation is relatively large, reducing accumulation over the land ice sheet [*Gildor and Tziperman*, 2000].

4. Sensitivity Study

[44] In this section we verify that the switch-like growth of sea ice is not affected by model resolution nor by the specific rate of land ice growth used in our experiments. Readers less interested in this technical material may skip directly to the conclusions.

4.1. Sensitivity to Model Resolution

[45] To explore this sensitivity, we first halved and then doubled the model's meridional resolution from our standard 3° per cell and ran it with the initial condition corresponding to the middle temperature profile in Figure 4 (IC 2, Table 5). The relative areas of land and ocean out of
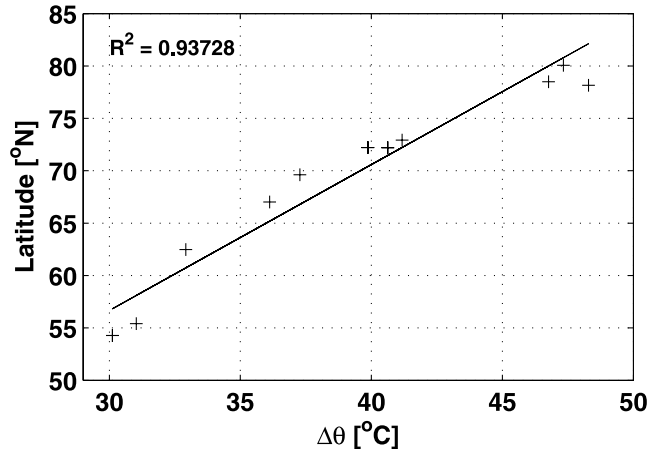

Figure 7. Extent of switch-like sea ice growth (vertical axis, in degrees) versus the initial atmospheric temperature gradient in °C (horizontal axis). The extent of switch-like sea ice growth is defined to be the southernmost latitude with sea ice immediately after the switch-like sea ice expansion. Each plus sign marks an experiment with different initial meridional temperature gradient (including those that appear in Table 6), while the solid line is a linear fit. The sea ice extent plotted here is calculated, for all model runs, 1000 years after the continental ice sheet had reached its threshold value and sea ice started growing.

the total surface were kept constant as the resolution was varied and so were the initial dimensions (surface and volume) of the ice sheets. The doubling of the model's spatial resolution demanded halving of the atmospheric time step to keep the model stable. Besides this change, all other model parameters remained the same.
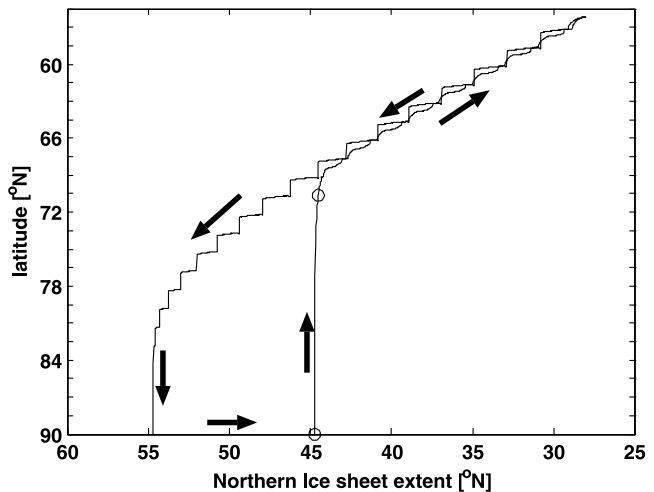

Figure 8. Hysteresis between the land ice extent (horizontal axis) and sea ice extent (vertical axis). Extent of both sea ice and land ice is defined as the southernmost latitude with sea or land ice, respectively. This plot was obtained by slowly increasing and then decreasing the land ice volume using the 1.5° resolution version of the coupled model. Circles denote beginning and end of sea ice growth, as in Figure 5.
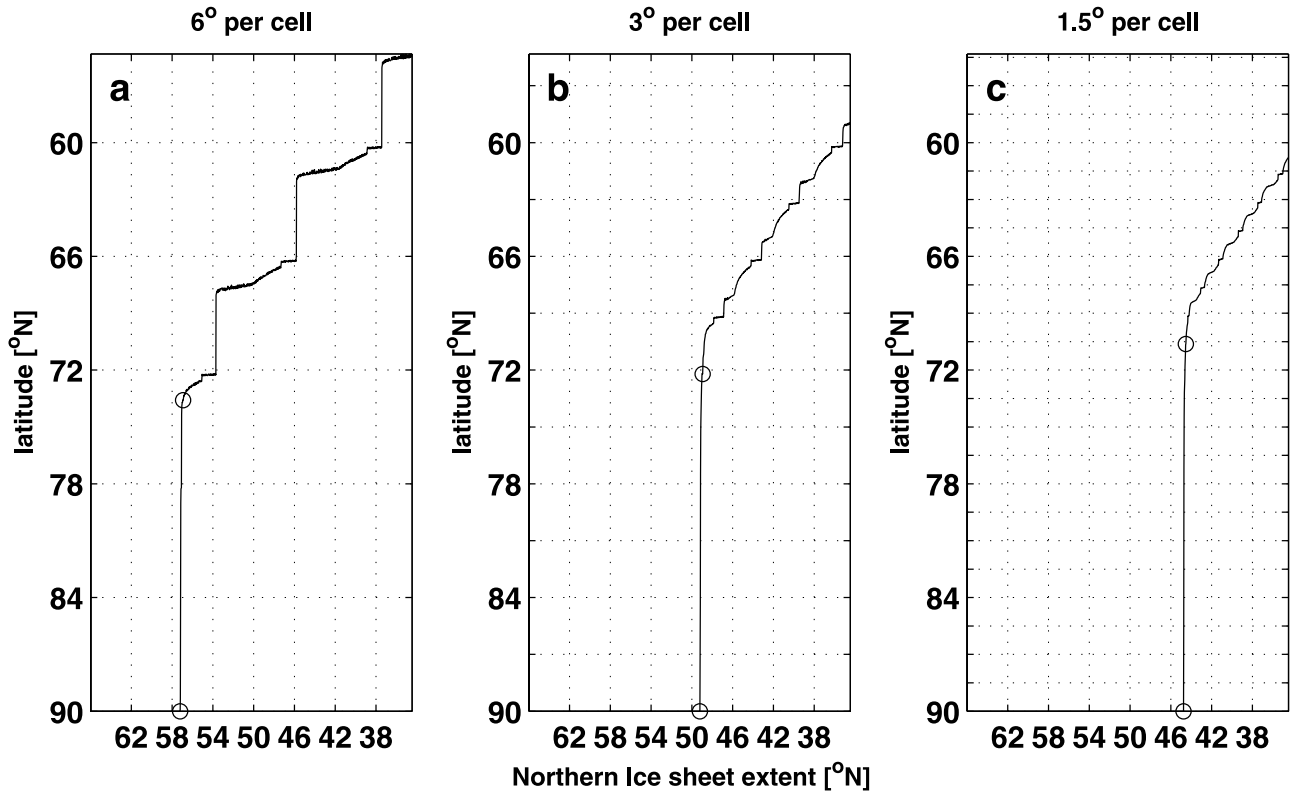
Figure 9. Plots of the sensitivity to model resolution. Shown is the sea ice extent as a function of slowly increasing land ice sheets for model runs with meridional resolutions of (a) 6°, (b) 3°, and (c) 1.5° per cell. Besides the atmospheric time step that is halved in the higher-resolution experiments to keep the model stable, all other model parameters and initial conditions are the same for all three runs. The horizontal axis shows the latitude of the southernmost edge of the northern ice sheet. The vertical axis shows the southernmost latitude with sea ice in the Northern Hemisphere. The circles indicate the beginning of the sea ice growth and a time mark of 1000 years later. The switch-like sea ice growth and its meridional extent (the distance between the two circles) are clearly very similar for all three resolutions. The threshold value of the continental ice sheet extent which triggers sea ice growth does seem sensitive to the meridional resolution.

[46] Figure 9 shows that the switch-like growth of the Northern Hemisphere sea ice remains practically unchanged for all three model resolutions. The extent of the sea ice switch-like growth is between 70.5°N and 73.5°N for all three resolutions examined. This growth occurs in all runs within a period of ~1000 years. The rate at which sea ice grows beyond the switch-like phase is also similar at all resolutions, although the step-like pattern at that stage looks different at the different resolutions. It should be emphasized again that sea ice is allowed to expand continuously in the latitudinal direction within each grid cell. As soon as sea ice appears in a given latitudinal band, it can therefore continuously expand to the next equatorward band.

[47] The main characteristics of the switch-like sea ice growth are clearly not sensitive to model resolutions of between 6° and 1.5°. On the other hand, the critical land ice cover that triggers the sea ice growth does seem to be sensitive to the latitudinal resolution. Sea ice growth switches "on" when the northern continental ice extent

reaches 57°N, 49°N, and 45°N for the meridional resolutions of 6°, 3°, and 1.5° per cell, respectively. Given the sensitivity of the critical land ice extent to the THC, the latter could have been a candidate explanation for the sensitivity to the resolution. However, it turns out that the THC is not sensitive to the model resolution in these runs. We must therefore submit that a satisfying explanation for this sensitivity to resolution is still missing. This is certainly a reason for concern, although we do feel that we have demonstrated that the switch-like sea ice growth and the land ice versus sea ice hysteresis are at least qualitatively robust features that are not sensitive to model resolution or parameters.

4.2. Sensitivity to the Rate of Land Ice Growth (LI$_{source}$)

[48] To check whether our results are insensitive to the specified rate at which the land ice volume increases (LI$_{source}$), we compared runs with land ice growth rates of 25, 12.5, and 6.25×10^4 m^3 s^{-1} (equivalent to a 195, 97.5,

and 48.75 m per 10,000 year reduction rate in real ocean level, respectively) in which the northern ice sheet grows from the same initial extent of 65°N south to 30°N. The sea ice response in all three runs remained the same in both meridional extent and volume (not shown but see *Sayag* [2003]). The results presented in this paper are thus insensitive to a wide regime of ice sheet growth rates.

5. Conclusions

[49] We examined the rapid, switch-like growth of sea ice under a specified slow climate cooling, as well as the sea ice–land ice hysteresis, in a simple, zonally averaged coupled model that is continuous in the latitudinal direction. The three major issues examined in this model were the extent to which the sea ice expanded rapidly in a switch-like manner, the minimal ice sheet cover needed to trigger the sea ice growth, and the existence of a hysteresis between the land ice and sea ice.

[50] We found that sea ice indeed grows in a switch-like manner even for a model with a continuous resolution of the meridional temperature gradient in the ocean and atmosphere. This supports the results of *Gildor and Tziperman* [2000], who used a model with a single surface ocean box and a single surface ocean temperature from 45°N to the pole. Next, we found that the meridional extent to which sea ice grows during its switch-like growth stage depends linearly on the initial meridional atmospheric temperature gradient. That is, a smaller initial temperature gradient results in a larger extent to which the sea ice grows rapidly. This finding is very robust with respect to changes in the THC, the meridional atmospheric heat flux, and the atmospheric emissivity parameters.

[51] The THC intensity did not affect the extent of the switch-like sea ice growth, yet it was critical in determining the minimal ice sheet cover (and hence climate cooling) that permits the initiation of sea ice growth. The meridional atmospheric heat flux had a similar effect. A larger meridional heat flux due to a stronger THC or a larger atmospheric meridional heat flux required larger land ice extent to trigger the sea ice growth. We also showed that switch-like sea ice growth is insensitive to the meridional model's resolution.

[52] Finally, we obtained in our continuously resolved model the same hysteresis between sea ice and land ice (Figure 8) that was predicted for the glacial cycles by *Gildor and Tziperman* [2000]. This is perhaps the element of the sea ice switch mechanism that is the most accessible to verification in the near future using new sea ice proxies that are becoming available [*DeVernal et al.*, 2000; *Sarnthein et al.*, 2003].

[53] Our model was clearly oversimplified. The model physics is simple, the geometry is rectangular, and some of the interactions of Northern Hemisphere sea ice with other climate components such as the Southern Hemisphere ice sheet and sea ice are absent. These simplifications were chosen in order to allow an in-depth process study of the sea ice switch-like behavior in isolation from other phenomena. The model described in this paper is, nevertheless, still a step forward relative to previous works in terms of latitudinal resolution. Yet more realistic physics and geometry are needed in future work.

References

Adams, J., M. Maslin, and E. Thomas (1999), Sudden climate transitions during the Quaternary, *Prog. Phys. Geogr.*, *23*(1), 1–36.

Bond, G., et al. (1992), Evidence for massive discharges of icebergs into the North Atlantic Ocean during the last glacial period, *Nature*, *360*, 245–249.

Broecker, W. (2000), Abrupt climate change: Casual constraints provided by the paleoclimate record, *Earth Sci. Rev.*, *51*, 137–154.

Bryan, K., S. Manabe, and R. Pacanowski (1974), A global ocean-atmosphere climate model. part 2. The oceanic circulation, *J. Phys. Oceanogr.*, *5*(1), 30–46.

Crowley, T. J., and G. R. North (1991), *Paleoclimatology*, 339 pp., Oxford Univ. Press, New York.

Dansgaard, W., S. J. Johnsen, H. B. Clausen, D. Dahl-Jensen, N. Gundestrup, C. U. Hammer, and H. Oescger (1984), North Atlantic climate oscillations revealed by deep Greenland ice cores, in *Climate Processes and Climate Sensitivity*, *Geophys. Monogr. Ser.*, vol. 5, edited by J. E. Hansen and T. Takahashi, pp. 288–298, AGU, Washington, D. C.

Dansgaard, W., J. White, and S. Johnsen (1989), The abrupt termination of the Younger Dryas climate event, *Nature*, *339*, 532–534.

DeVernal, A., C. Hillaire-Marcel, J. L. Turon, and J. Matthiessen (2000), Reconstruction of sea-surface temperature, salinity, and sea-ice cover in the northern North Atlantic during the last glacial maximum based on dinocyst assemblages, *Can. J. Earth Sci.*, *37*(5), 725–750.

Ganopolski, A., and S. Rahmstorf (2001), Rapid changes of glacial climate simulated in a coupled climate model, *Nature*, *409*, 153–158.

Ghil, M. (1994), Cryothermodynamics: The chaotic dynamics of paleoclimate, *Physica D*, *77*, 130–159.

Ghil, M., and H. L. Treut (1981), A climate model with cryodynamics and geodynamics, *J. Geophys. Res.*, *86*(C6), 5262–5270.

Gildor, H., and E. Tziperman (2000), Sea ice as the glacial cycles' climate switch: Role of seasonal and orbital forcing, *Paleoceanography*, *15*(6), 605–615.

Gildor, H., and E. Tziperman (2001), A sea-ice climate-switch mechanism for the 100 kyr glacial cycles, *J. Geophys. Res.*, *106*(C5), 9117–9133.

Gill, A. E. (1982), *Atmosphere-Ocean Dynamics*, 662 pp., Academic, San Diego, Calif.

Haltiner, G. J., and R. T. Williams (1980), *Numerical Prediction and Dynamical Meteorology*, John Wiley, Hoboken, N. J.

Heinrich, H. (1988), Origin and consequences of cyclic ice rafting in the northeast Atlantic Ocean during the past 130,000 years, *Quat. Res.*, *29*, 142–152.

Huang, R. H., J. R. Luyten, and H. M. Stommel (1992), Multiple equilibrium states in combined thermal and saline circulation, *J. Phys. Oceanogr.*, *22*(3), 231–246.

Kerr, R. A. (2002), Mild winters mostly hot air, not Gulf Stream, *Science*, *297*, 2202.

Marotzke, J. (2000), Abrupt climate change and thermohaline circulation: Mechanisms and predictability, *Proc. Natl. Acad. Sci. U.S.A.*, *97*, 1347–1350.

Marotzke, J., and P. H. Stone (1995), Atmospheric transports, the thermohaline circulation, and flux adjustments in a simple coupled model, *J. Phys. Oceanogr.*, *25*(6), 1350–1364.

Paterson, W. (1994), *The Physics of Glaciers*, 3rd ed., 480 pp., Pergamon, New York.

Peixoto, J., and A. Oort (1991), *Physics of Climate*, Am. Inst. of Phys., College Park, Md.

Rivin, I., and E. Tziperman (1997), Linear versus self-sustained interdecadal thermohaline variability in a coupled box model, *J. Phys. Oceanogr.*, 27(7), 1216–1232.

Sarnthein, M., U. Pflaumann, and M. Weinelt (2003), Past extent of sea ice in the northern North Atlantic inferred from foraminiferal paleotemperature estimates, *Paleoceanography*, 18(2), 1047, doi:10.1029/2002PA000771.

Sayag, R. (2003), Rapid switch-like sea ice growth and land ice–sea ice hysteresis in a continuous coupled model, M.S. thesis, Weizmann Inst., Rehovot, Israel.

Seager, R., D. S. Battisti, J. Yin, N. Gordon, N. Naik, A. C. Clement, and M. A. Cane (2002), Is the Gulf Stream responsible for Europe's mild winters?, *Q. J. R. Meteorol. Soc.*, 128, 2563–2586.

Stommel, H. (1961), Thermohaline convection with two stable regimes of flow, *Tellus*, 13, 224–230.

Stone, P. H. (1990), Development of a 2-dimensional zonally averaged statistical-dynamic model. 3. The parameterization of the eddy fluxes of heat and moisture, *J. Clim.*, 3, 726–740.

Trenberth, K., and J. Caron (2001), Estimates of meridional atmosphere and ocean heat transports, *J. Clim.*, 14, 3433–3443.

Tziperman, E. (1997), Inherently unstable climate behaviour due to weak thermohaline ocean circulation, *Nature*, 386, 592–595.

Tziperman, E., J. R. Toggweiler, K. Bryan, and Y. Feliks (1994), Instability of the thermohaline circulation with respect to mixed boundary conditions: Is it really a problem for realistic models?, *J. Phys. Oceanogr.*, 24(2), 217–232.

Weaver, A. J., E. S. Sarachik, and J. Marotzke (1991), Freshwater flux forcing of decadal and interdecadal oceanic variability, *Nature*, 353, 836–838.

————————————

M. Ghil, Département Terre-Atmosphère-Océan and Laboratoire de Météorologie Dynamique, Ecole Normale Supérieure, 24, rue Lhomond F-75231 Paris Cedex 05, France. (michael.ghil@lmd.ens.fr)

R. Sayag and E. Tziperman, Earth and Planetary Sciences, Harvard University, 20 Oxford St., Cambridge, MA 02138-2902, USA. (sayag@fas.harvard.edu; eli@eps.harvard.edu)